Solar Energy Materials and Solar Cells 200 (2019) 109981

Contents lists available at ScienceDirect

Solar Energy Materials and Solar Cells

journal homepage: www.elsevier.com/locate/solmat

Contactless determination of base resistivity on silicon wafers with highly doped surfaces

Hannes Höffler*, Andreas A. Brand, Wiebke Wirtz, Johannes Greulich

Fraunhofer Institute for Solar Energy Systems ISE, Heidenhofstr. 2, D-79110, Freiburg, Germany

ARTICLE INFO

Keywords:
Silicon
Characterization
Conductivity
Photoluminescence
Sheet resistance

ABSTRACT

In this paper a contactless and non-destructive method for the determination of base resistivity of silicon wafers with highly doped surfaces is introduced. The method is based on photoconductance and photoluminescence measurements. Unlike existing methods for the determination of base resistivity, the proposed method does not require an experimental setup, which simultaneously measures photoconductance and photoluminescence signals synchronized in time. The method is applied to a set of test samples with highly doped surfaces representing a broad variety of samples present in industrial and laboratory environments. The results of the proposed method are compared to reference values which are inductively measured after the removal of highly doped surfaces. An mean absolute error with respect to the reference values below 4% is obtained for the investigated set of samples. This corresponds to a deviation of less than 0.1 Ωcm for typical solar wafers with resistivities below 5 Ωcm. Sources of uncertainties in the proposed method are discussed in detail. From that discussion rules of thumb for a reasonable choice of calibration and test samples are derived. A maximum error of less than 10% is expected if rules of thumb are followed.

1. Introduction

In solar energy research laboratories solar cell precursors are important vehicles for process development and optimization. The term 'solar cell precursors' is not strictly defined, but in most cases solar cell precursors feature highly doped surfaces at least one side. Since the base resistivity of solar cell precursors is often not accurately specified by suppliers and resistivity may change during high temperature processes, a measurement method for the base resistivity of solar cell precursors is highly desirable. Established methods like four-point-probe (4pp) measurements or inductive (eddy-current) measurements [1] are not applicable to wafers with highly doped surfaces because the 4pp-technique measures the sheet resistance of the highly doped layer only - if a pn-junction is present - and the inductive measurement determines the parallel resistance of the base and the highly doped surface. By a combination of 4pp and inductive measurements the base resistivity can be determined, but nonetheless this is an approach, which is damaging the wafer surfaces. A non-destructive method, which is based on the simultaneous detection of a photoconductivity (PC) and a photoluminescence (PL) signal has already been proposed by Hameiri et al. [2]. Although the method proposed in [2] is very elegant and excellently verified, it requires the availability of a PC measurement setup, which simultaneously measures the PL signal and the PC signal of the sample at low and high level injection conditions. In many research laboratories only separate photoluminescence imaging (PLI) and PC setups are available, PLI measurements are not necessarily available in high level injection and the measurements are not synchronized in time.

In this paper we propose a contactless and non-destructive method (here named PLI-PC method) for the determination of base resistivity of wafers with highly doped surfaces, which does not require the availability of a setup, which simultaneously measures the PC and the PL signal and does not necessarily need light sources inducing high level injection conditions. The method is based on the combination of PLI [3] and PC measurements [4].

After the PLI-PC method is introduced, it is applied to a set of test samples representing a broad variety of base resistivities and optical properties. The base resistivity determined by the PLI-PC method is compared to results determined by inductive measurements after the removal of the highly doped layers. A detailed error analysis is conducted, which identifies the dominating errors, and suggests a correction method.

2. Theory of the PLI-PC method

From the well-established theory about photoluminescence of

* Corresponding author.
E-mail address: hannes.hoeffler@ise.fraunhofer.de (H. Höffler).

https://doi.org/10.1016/j.solmat.2019.109981
Received 4 April 2019; Received in revised form 31 May 2019; Accepted 2 June 2019
Available online 12 June 2019
0927-0248/

silicon wafers [5,6] it can be derived that the detected PL signal ϕ is correlated to the rate of spontaneous recombination per wavelength interval $r_{ph}(\lambda)$ via:

$$\phi = \int_0^\infty \int_0^W f_{det}(\lambda) \cdot f_{esc} \cdot (\lambda, z) \cdot r_{ph}(\lambda, z) \mathrm{d}z \mathrm{d}\lambda \tag{1}$$

Here $f_{det}(\lambda)$ is the detection probability of a photon with wavelength λ, which escaped the sample, $f_{esc}(\lambda, z)$ is the escape probability for a photon generated within the sample in the depth z, and W is the sample thickness. The detection probability can be split up into a constant factor K, in which all non-wavelength dependent setup specific effects are lumped, and into a wavelength dependent part, which is the product of the transmittance of the optical filters located before the detector $T_f(\lambda)$ and the detectors quantum efficiency $QE_{\mathrm{det}}(\lambda)$ [7].

$$f_{det}(\lambda) = K \cdot T_f(\lambda) \cdot QE_{\mathrm{det}}(\lambda) \tag{2}$$

The escape probability depends on the optical properties of the sample and the sample's thickness. For optically rough surfaces f_{esc} can be a complicated function of reflectivity and roughness parameters [8], which in general cannot be accessed experimentally in an easy way. A simplified approach [9,10], which nevertheless is only valid for planar surfaces, gives f_{esc} as a function of front and rear reflectivity. In a strongly simplified approach internal rear reflectivity and the role of internal front reflectivity is completely neglected and only reabsorption is taken into account. This approach is followed in this work and motivated if a short-pass filter is used in the experimental setup in front of the detector, which blocks wavelengths larger than 1000 nm. For wavelengths below 1000 nm the penetration depth in silicon is below 160 µm. Neglecting internal front and rear reflection and the escape probability can be written as:

$$f_{esc}(z, \lambda) \propto \mathrm{e}^{-\alpha(\lambda) \cdot z} \tag{3}$$

where α is the absorption coefficient of silicon [11]. The spontaneous recombination rate $r_{sp}(\lambda, z)$ is proportional to the product of electron and hole densities n and p, if doping and injection dependence of the coefficient of radiative recombination [12] are neglected

$$r_{sp}(\lambda, z) \propto \frac{\alpha(\lambda) \cdot n(z) \cdot p(z)}{\lambda^4 \cdot \exp \frac{h \cdot c}{\lambda \cdot k \cdot T}} \tag{4}$$

Here h, c, k and T are the Planck constant, the speed of light, the Boltzmann constant and the temperature respectively. If we neglect reabsorption, internal reflection and assume that the carrier densities do not depend on the depth for a moment, then f_{esc} and r_{sp} become depth-independent and equation (1) hugely simplifies to:

$$\phi = a \cdot W \cdot n \cdot p. \tag{5}$$

Here a is a calibration factor, which is *not* sample specific and the only sample specific property, which relates the luminescence signal to the carrier densities is the sample thickness. The assumptions leading to the simplification are discussed below. The great advantage of this simplification is that the thickness can be accessed experimentally in a very easy way. Introducing the excess carrier density Δn and the doping density N_{dop} equation **(5)** can be rewritten as:

$$\phi = a \cdot W \cdot \Delta n \cdot (\Delta n + N_{dop}). \tag{6}$$

If a and Δn at a certain generation rate are known the doping density and hence the base resistivity can be calculated by measuring the PL-signal ϕ. The most critical assumption in the derivation of equation **(6)** is neglecting reabsorption. If the detector would detect photons homogeneously throughout the whole depth of the wafer, neglecting reabsorption would be perfectly fine. Nevertheless the luminescence radiation with wavelengths shorter than 1000 nm only has penetration depths lower than 160 µm which is in the order of typical wafer thicknesses. For this reason, the thickness can neither be neglected nor be included linearly into equation **(6)**. Reabsorption can be taken into account more realistically if the thickness W in equation **(6)** is replaced by a thickness weighting function $f(W)$, which is the thickness itself for very thin samples and converges against a constant value for very thick samples. Equation **(6)** then writes:

$$\phi = a \cdot f(W) \cdot \Delta n \cdot (\Delta n + N_{dop}). \tag{7}$$

As equation **(7)** represents the central equation of the PLI-PC approach details on the determination of every quantity in equation **(7)** are given in the following.

2.1. Determination of Δn

The excess carrier density Δn in equation **(7)** is determined via PC measurements. The most commonly distributed setup to conduct PC measurements on silicon wafers is the commercially available Sinton Instruments lifetime tester WCT-120, which is also used in this work. Simply speaking, the PC measurement setup measures $\Delta n(t)$ and the generation rate $G_{\mathrm{flash}}(t)$ in the sample. According to the continuity equation the recombination rate R can be calculated via $R(t) = G_{\mathrm{flash}}(t) - \frac{\partial \Delta n(t)}{\partial t}$ [13]. Hence the PC measurement results can be interpreted as excess carrier density as function of recombination rate $\Delta n(R)$. The PL setup measures the PL intensity ϕ and the photon flux j_{ph} arriving onto the cell. If the PL images are taken under steady state conditions, which is always the case in this work, the recombination rate R_{PLI} during the PL image acquisition is equal to the generation rate G_{PLI} while the wafer is excited by illumination during the PLI measurement. The generation rate G_{PLI} calculates via $G_{PLI} = \frac{j_{ph} \cdot (1 - R_{f,808})}{W} = R_{PLI}$, where $R_{f,808}$ is the external front side reflectance of the sample at 808 nm. (The PLI-setup used in this work uses monochromatic excitation light of 808 nm) The excess carrier density $\Delta n(R_{PLI})$, which has to be inserted into equation **(7)**, is the excess carrier density at the point where the recombination rate R during the PC measurement is equal to the recombination rate R_{PLI} during the PL-imaging measurement. It should be noted that complete absorption of excitation light is necessary in order to calculate G_{PLI}. If excitation wavelength of PLI setups are larger than 940 nm (penetration depth $>$ 50 µm) and wafers are extremely thin, this might become an issue.

The essential idea of the PLI-PC method is that $\Delta n(R_{PLI})$ can be determined by the PC measurement *without* the exact knowledge of the doping concentration N_{dop}. One might argue that N_{dop} is a necessary input parameter in the PC-measurement, which is needed to determine the carrier mobility. Nevertheless, this problem can be circumvented by an iterative procedure, which is explained below, because carrier mobilities only depend weakly on N_{dop}.

2.2. Determination of ϕ

The PL signal ϕ is extracted from the PL image. It is important that the PL signal at the correct position is considered here, so one cannot take any arbitrary mean value of the image. The PL signal has to be considered at the position where the PC measurement is conducted. Hence the PL signal ϕ has to be the mean of the measured PL image weighted over the coil response function of the PC measurement setup. For the commercially available WCT-120 setup used in this work different coil response functions are published in literature [14–16] and their validity is discussed in [15]. In this work we assume the coil response function suggested in [16], where the coil response function is represented by a Gaussian ring with radius 9.3 mm and width 3.6 mm. The validity can be questioned, but uncertainties in the coil response function within reasonable limits are negligible for the method proposed in this work, which is discussed below.

2.3. Determination of the calibration factor a

The determination of the calibration factor is the most critical part of the proposed method. The calibration factor of the calibration wafer a_{CW} is determined by measuring a calibration wafer or ideally a set of calibration wafers with *known* base resistivity with the PLI and the PC setup in use. Transforming equation **(6)** a_{CW} then reads:

$$a_{CW} = \frac{\phi_{CW}}{f(W_{\mathrm{CW}})\cdot\Delta n(R_{PLI})\cdot(N_{dop,\mathrm{CW}} + \Delta n(R_{PLI}))} \tag{8}$$

where W_{CW} and $N_{dop,\mathrm{CW}}$ are thickness and doping density of the calibration wafer respectively. $f(W_{\mathrm{CW}})$ denotes the thickness weighting function which is discussed below. The PL signal ϕ_{CW} in equation (8) is the signal of the measured PL image weighted over the coil response function of the PC measurement setup. Assuming similar optical properties and no depth dependence of carrier concentrations, the calibration factor of the test wafer a_{test} and a_{CW} are then simply be assumed to be equal.

2.4. Calculation of the thickness weighting function $f(W)$

As discussed above the wafer thickness can neither be neglected nor be included linearly as done in equation **(6)**. To calculate the thickness weighting function $f(W)$ used in equation **(7)** it is necessary to know the filter transmittance $T_f(\lambda)$ and the detector's quantum efficiency $QE_{\mathrm{det}}(\lambda)$ of the PLI setup in use. The weighting function can then be calculated via:

$$f(W) = \frac{\int_0^W \int_0^\infty T_f(\lambda)\cdot QE_{\mathrm{det}}(\lambda)\cdot \frac{\alpha(\lambda)}{\lambda^4\cdot\exp\frac{h\cdot c}{\lambda\cdot k\cdot T}}\cdot \mathrm{e}^{-\alpha(\lambda)\cdot z}\mathrm{d}\lambda\mathrm{d}z}{f(1\ \mu\mathrm{m})} \tag{9}$$

The denominator $f(1\ \mu\mathrm{m})$ is only introduced for convenience here to scale the function such that it equals the thickness itself for 1 µm. It can be left out without limitation of generality. Equation **(9)** can be understood the following way: The weighting function is supposed to cancel out the differences in PL-signal, which are only thickness related. The PL-signal ratio of two wafers with equal carrier density products but different thicknesses would result in the ratio of the two thickness weighting functions, as can be derived directly from equation **(1)** to **(4)**. The weighting function is a setup specific property, which can in practice be changed by changing filters in front of the detector or the detector itself. Weighting functions for three different setup scenarios are illustrated in Fig. 1.

As can be observed from Fig. 1 the weighting function depends on the different setup scenarios. If the long wavelength part of the luminescence spectrum is fully detected (orange dotted line), the detector 'sees through' the whole wafer and thickness would have to be included almost linearly like proposed in equation **(6)**. The setup used in this work is equipped with a 1000 nm short pass filter in addition to the long pass filters, that are necessary to block excitation light. For the case of the setup used in this work (green solid line) the thickness needs to be weighted in a correct manner. The weighting function corresponding to the green solid line is used in all calculations in this work. Note that the weighting function is only important if thicknesses of calibration and test wafer are different. If thicknesses are similar or equal $f(W)$ can be ignored and no detailed knowledge about the properties of the PLI setup is necessary. It should be noted that equation **(9)** assumes no internal reflection of PL-radiation within the wafer.

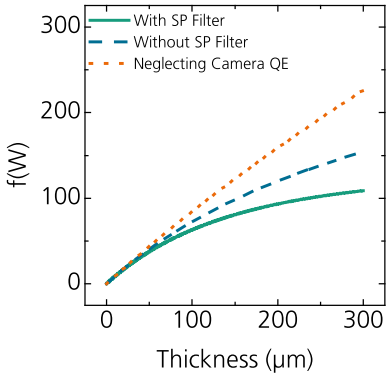

Fig. 1. Weighting function for three different scenarios. 1.) Using filter transmittances from the PLI-setup used in this work (green solid line). 2.) Assuming no short pass (SP) filters (blue dashed line). 3.) Neglecting wavelength dependent quantum efficiency of detector (orange dotted line). (For interpretation of the references to color in this figure legend, the reader is referred to the Web version of this article.)

2.5. Determination of doping density N_{dop} and base resistivity ρ

After the determination of the excess carrier density at the recombination rate during the PLI measurement $\Delta n(R_{PLI})$ and the determination of the calibration constant of the wafer under test a_{test} the doping density of the wafer under test can easily be determined from equation **(7)**

$$N_{dop} = \frac{\phi_{\mathrm{test}}}{a_{\mathrm{test}}\cdot f(W_{\mathrm{test}})\cdot\Delta n(R_{PLI})} - \Delta n(R_{PLI}) \tag{10}$$

where ϕ_{test} is the luminescence signal of the test wafer weighted over the coil response function. As a general remark it should be noted at this stage that it is highly recommended to be at low or intermediate injection conditions during the PLI measurements. If Δn becomes much larger than N_{dop} the term N_{dop} can be neglected in the sum of equation **(7)**, which would cause the method to fail. The base resistivity and the doping density relate via:

$$\rho = \frac{1}{q\cdot N_{dop}\cdot\mu_{n/p}} \tag{11}$$

where q is the elementary charge, and $\mu_{n/p}$ is the mobility of majority carriers, i.e. electrons or holes depending on the type of the material. The mobilities are a function of doping density themselves, which is discussed in [17] and various other publications summarized in [18]. It should be mentioned that the PLI-PC method measures the net base doping concentration. Due to the presence of thermal donors [19] for example the net base doping concentration could change after high temperature processing steps.

2.6. Iterative adoption of mobilities

As mentioned above one might argue that the knowledge of the base resistivity is necessary for the PC measurement to take mobility changes into account. This can be circumvented by iterating the evaluation of the PC raw data and the PLI-PC approach. The PC measurement of the sample under test with unknown base resistivity can be done with any reasonable starting value for the base resistivity (in this work 1 Ωcm is used). The conductivity difference $\Delta\sigma$ measured by the PC measurement setup does *not* depend on the assumed base resistivity. The excess carrier density Δn, which is needed for the determination of base resistivity in the PLI-PC approach is (as described in [20]) calculated using:

$$\Delta n = \frac{\Delta\sigma}{q\cdot W\cdot(\mu_n(\rho) + \mu_p(\rho))} \tag{12}$$

Although the mobilities in equation **(12)** depend on the base resistivity themselves, one can firstly use equation **(12)** with the mobilities corresponding to the assumed starting values. This will yield a first set of excess carrier densities $\Delta n_{1\mathrm{st}}$, and hence a first value of base resistivity $\rho_{1\mathrm{st}}$ can be determined by the PLI-PC method. In a second iteration mobility values corresponding to $\rho_{1\mathrm{st}}$ are chosen and a second

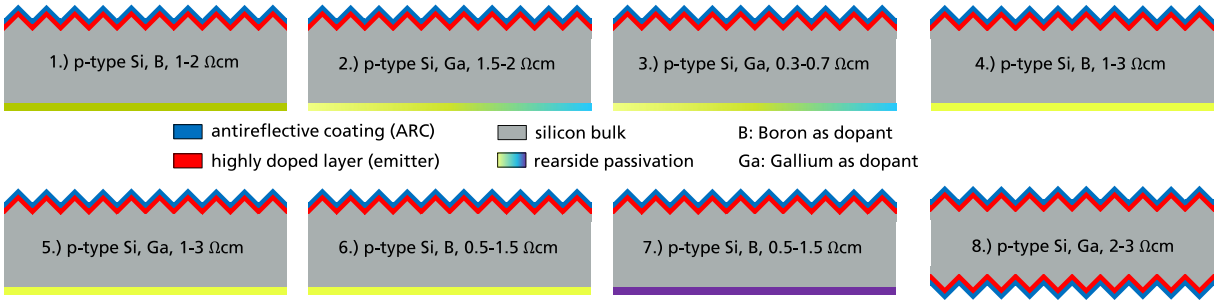

Fig. 2. Schematic representation of the selected sample set (28 samples, 8 groups). The rear side color is chosen to roughly represent the color appearance to the eye. (For interpretation of the references to color in this figure legend, the reader is referred to the Web version of this article.)

set of excess carrier densities Δn_{2nd} is calculated using equation **(12)**. As shown in the experimental results below this iteration converges for every investigated sample. A satisfying convergence, resulting in less than 0.6 % deviation between the last two successive iteration steps, is reached after four iterations. Strictly speaking the mobilities also depend on the excess carrier density Δn. This can nevertheless be neglected in low level injection conditions.

3. Experiment and results

3.1. Design of experiment

To test the PLI-PC method described above a set of 28 test samples is selected. The selected sample set features eight groups, which are schematically depicted in Fig. 2.

All samples feature at least one highly doped surface (two in case of group 8), which makes the determination of base resistivity challenging. The samples are selected in order to represent a large variety of precursors that are used for process optimization in laboratory environments including PERC solar cell precursors. The samples stem from five different suppliers and feature different rear side passivation layers causing different optical properties (roughly represented by the varying colors in Fig. 2). The exact nature of the rear passivation layer is unknown and not of relevance for this work. Moreover a large variety (roughly 0.3–3 Ωcm) of base resistivities and sample thicknesses (130–190 µm) are chosen. Fig. 3 illustrates the measurements and processing steps conducted on the samples.

After sample selection the thickness and the total sheet resistance are measured capacitively and inductively with a commercially available system (MX 152 by E + H Metrology). 4pp-measurements are made from the front side with a commercially available system (TLM-Scan by PV-tools), which enables a prediction of base resistivity if combined with inductive measurement. After that the wafers are exposed to a high-temperature treatment in a fast firing oven (FFO-treatment) in order to activate the passivation layers. Resistivity changes originating from thermal donor anneal during the FFO-treatment are not expected, because the prior junction formation of each wafer already involves a high temperature step. After the FFO treatment PLI and PC measurements are conducted in order to enable a prediction of the base resistivity by the PLI-PC method (using a PLI setup developed by Fraunhofer ISE and a commercially available PC setup WCT-120 by Sinton Instruments). The PLI measurements are conducted under an irradiation of 0.1 suns ($2.5{\cdot}10^{16}\frac{\text{photons}}{\text{s}{\cdot}\text{cm}^2}$) in order to assure low injection levels. Additionally the spectrally resolved reflectance is measured for each sample using a commercially available system (LOANA by PV-tools). Subsequently the highly doped layers are chemically etched back by exposure to nitric acid (HNO_3) and hydrofluoric acid (HF) removing about 7–8 µm of silicon. After removing the highly doped layers, thickness and total sheet resistance are measured again. The base resistivity determined by the inductive measurement after the removal of highly doped layers is taken as a reference value, which can be compared to base resistivity predicted by PLI-PC and the prediction via combined 4pp and inductive measurements. Finally the calibration factor is determined by equation **(8)**. Hereby the 28 test wafers are treated as calibration wafers. The base resistivity determined after the removal of highly doped layers and the PL and PC results before the removal are inserted into equation **(8)**, which yields 28 calibration factors. The calibration factor a used in the following calculations is determined as the arithmetic mean of the 28 individual calibration factors. For this experiment a numerical value of $3.6{\cdot}10^{-26}\,\frac{\text{counts}}{\text{s}\cdot\text{cm}^6}$ was determined.

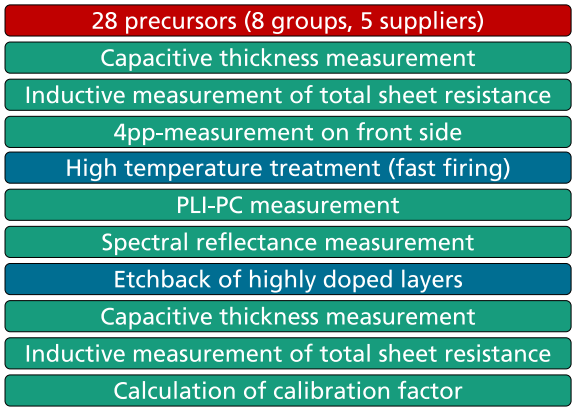

Fig. 3. Overview on measurement (green) and processing steps (blue) for the selected test samples. (For interpretation of the references to color in this figure legend, the reader is referred to the Web version of this article.)

4. Results

Fig. 4 a) shows the base resistivity determined by three different approaches on the set of test samples plotted against the reference values determined inductively after the removal of highly doped layers. The green squares represent the base resistivities determined by the PLI-PC approach without the iterative mobility adoption described in section 2 using a value of 1 Ωcm as input for the PC measurement for every wafer. The blue circles represent the base resistivity values determined by PLI-PC using the iterative adoption of mobilities (four iterations were sufficient and converged for every investigated sample). The yellow inverted triangles represent the values obtained by measuring the sheet resistance $R_{sh,4pp}$ of the highly doped layer via 4pp and the total sheet resistance $R_{sh,tot}$ via inductive measurements. The base resistivity ρ_{comb} of this combined method is then calculated via $\rho_{comb} = \left(\frac{1}{R_{sh,tot}} - \frac{n}{R_{sh,4pp}}\right)^{-1}\cdot W$, where n is the number of highly doped layers (2 in case of group 8).

Fig. 4 b) shows the distribution of the deviations to the reference values determined after the removal of highly doped layers. The combination of 4pp and inductive measurements before the removal of

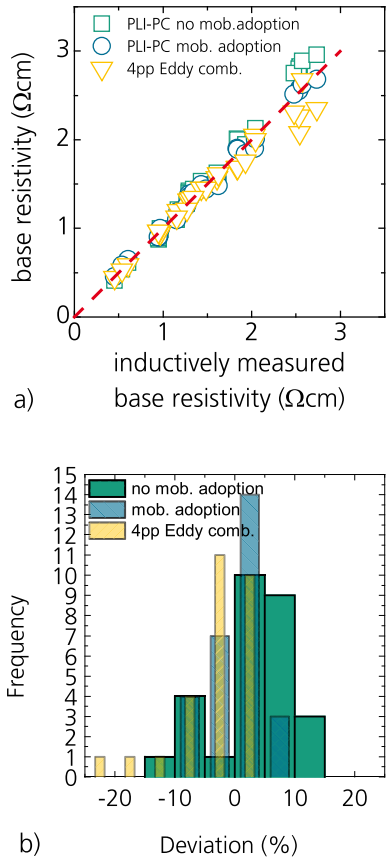

Fig. 4. a): Base resistivity determined by the PLI-PC approach after high temperature treatment with and without iterative mobility adoption and base resistivity determined by combined 4pp and inductive measurement plotted against the base resistivity determined inductively after removal of highly doped surfaces. b): Deviations of values determined by PLI-PC and combined 4pp and inductive measurement to the inductively determined reference values.

highly doped layers shows good agreement. The mean absolute error (MAE) to the reference values is 4.4 %. The three outliers suffering from more than 10 % deviation all belong to group 8, which features 2 highly doped surfaces. Nevertheless the 4pp measurement possibly causes damage or contamination of the wafers, which strongly motivates the PLI-PC method. If the mobility adoption proposed in section 2 is not applied the PLI-PC approach shows a MAE of 5.6 % from the reference values. If the mobility adoption is applied the PLI-PC approach shows excellent agreement with a MAE of 3.6 % to the reference values and maximum deviations are below 10 % for every investigated sample.

5. Error analysis and accuracy of PLI-PC

As can be seen in Fig. 4 b) there are still deviations from the base resistivity obtained from the PLI-PC method to the reference method. The most drastic simplification used by the PLI-PC method is that the calibration factor a is assumed to be the same for every sample under test and for the calibration samples. This is a valid assumption if all samples' optical properties and the depth-dependence of the charge carrier profile are similar. In order to demonstrate the validity of this assumption the distribution of the 28 individual calibration constants of the sample set relative to their mean is shown in Fig. 5 a).

It can be seen that the calibration constants deviate up to 20 % from each other for the extreme cases. An error in the calibration constant propagates directly to the base resistivity determined by the PLI-PC approach. Fig. 5 b) shows the imperfect correlation of the detected luminescence signal to the product of thickness weighting function, measured excess carrier density and the reference base doping

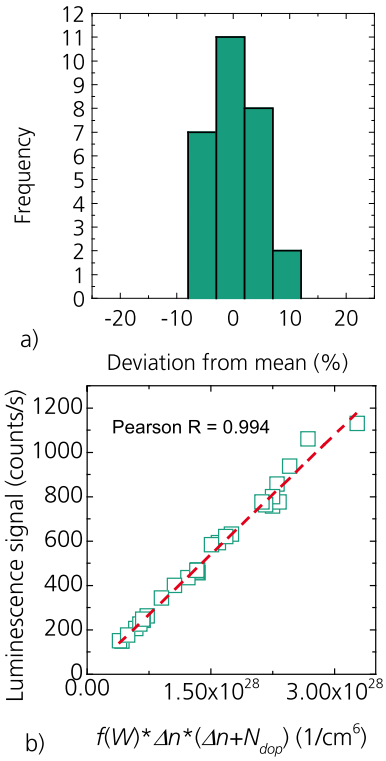

Fig. 5. a) Distribution of the individual calibration constants for the set of test wafers relative to their mean. b): Proportionality between the detected luminescence signal and the product of charge carriers and thickness.

determined by inductive measurement after the removal of highly doped layers. All sources of error in the PLI-PC approach directly show in the 'non-equality' of calibration factors. Several reasons can cause deviations of calibration constants between different samples. We split up the major reasons in three classes here and discuss them separately in the following.

- Optical differences between the samples (caused by different external and internal reflection properties of the samples)
- Depth dependent carrier concentrations
- Uncertainties in any other assumed quantities entering into the calculations (e.g. PC-coil response, PLI-detector sensitivity, parasitic effects increasing PLI-signal …)

In practice these three reasons cannot strictly be separated and can interfere with each other in complicated ways. Nevertheless for matters of clarity the reasons are discussed separately in the following.

5.1. Optical differences between samples

Optical differences between the samples will lead to different calibration factors. We perform a correlation analysis between the individual calibration constants of the 28 investigated samples and four optical parameters:

- External front transmittance at 800 nm
- External front transmittance at 1000 nm
- Internal front reflectivity
- Internal rear reflectivity

The four parameters are chosen because they are experimentally accessible and a correlation could be expected intuitively. The external front transmittance at 800 nm is directly calculated from the measured reflectance spectrum via $(1 - R_{f,\mathrm{ext}}(800\mathrm{nm}))$ with $R_{f,\mathrm{ext}}$ being the

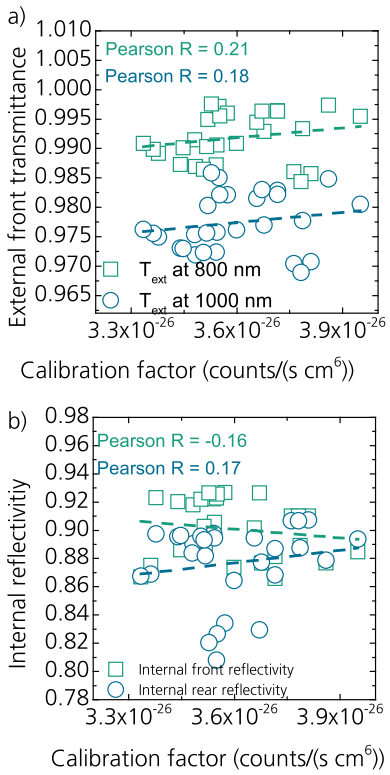

Fig. 6. a): Correlation between external front transmittances at 800 nm and 1000 nm and the individual calibration factors for the investigated samples. b): Correlation between the internal front and rear reflectivities extracted by fitting the reflectance spectra to an analytical model and the determined calibration factors for the investigated set of samples.

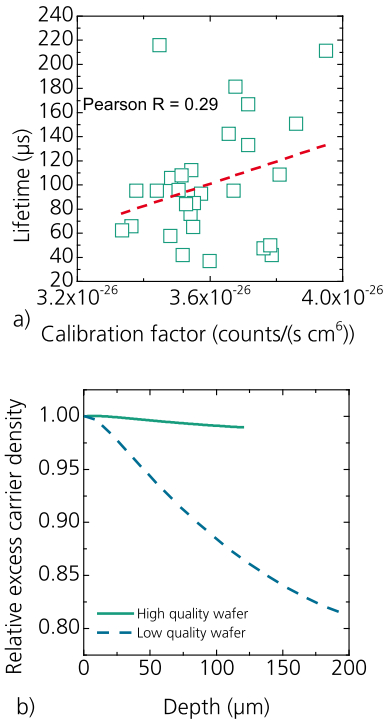

Fig. 7. a): Correlation between the calibration factor and the effective lifetime at the recombination rate during the PLI measurement measured before the etchback of highly doped layers. b): Simulated depth dependence of excess carrier concentrations for a 120 µm thick high quality wafer and a 200 µm thick low quality wafer.

external reflectance. The external reflectance at 1000 nm is calculated by fitting the part between 800 and 900 nm of the reflectance spectrum by a second order polynomial and the corresponding extrapolation as proposed in [21]. The internal front and rear reflectivities are extracted by fitting an analytical model similar to one suggested by Basore et al. in [22] to the measured reflectance spectrum. The correlation graphs of the four parameters to the determined calibration factors are shown in Fig. 6.

It can be seen that the Pearson coefficients do not exceed 0.21, which effectively indicates no correlation. This leads to the conclusion that neither of the four parameters are dominating the PLI-PC uncertainty in a clear way. There are in principle other parameters that have an impact on the escape probability [8], which are connected to surface roughness. Since these parameters cannot be excessed experimentally for the investigated samples, a comprehensive correlation analysis is beyond the scope of this work. It should be noted that in this work short pass filters in front of the detector are used during the acquisition of the PL images. This largely circumvents the problem of high sensitivity to the sample's internal optics as stated in [23]. Most of the light with wavelengths above 1000 nm is blocked and hence the impact of photons experiencing multiple bounces within the sample is low (PL light below 1000 nm features absorption lengths below 160 µm [11]). This argument and the correlation analysis above are not a proof but an indication for the fact that optical differences between the selected samples are not the dominating reason for differences in the calibration factors and hence not the dominating source of error in base resistivity prediction by PLI-PC. Note that this is specific for the chosen set of test samples. All samples feature an alkaline front side texture and an anti-reflection coating and hence have an optically similar front side. Comparing textured samples with planar samples would most probably lead to a significant impact of external front transmittance and internal reflectivity. Nevertheless this would be an unreasonable choice of samples, which can easily be avoided by checking the optical appearance of the samples.

5.2. Depth-dependent carrier concentration

Another reason for differences in the calibration factor of the calibration wafer and the test wafer is the presence of depth-dependent excess carrier concentrations $\Delta n(z)$ during the PLI measurement. Unfortunately the depth dependence of excess carriers cannot be accessed easily from experimental data. A first indication that depth dependence is not a major source of error is the missing correlation ($R = 0.29$) between minority carrier lifetime measured before etchback and calibration factor as shown in Fig. 7 a). Nevertheless this missing correlation is by no means a good proof for that fact.

In order to estimate the maximum error caused by the assumption of missing depth dependence, it makes sense to simulate the depth dependences of two extremely different samples. Excess carrier profiles for samples with known surface recombination velocities and bulk lifetimes can easily be simulated by analytical models such as proposed in [24], where surface recombination velocities and bulk lifetimes are assumed to be independent from injection level. We simulate the excess carrier profiles for a high quality sample featuring front and rear surface recombination velocities of $S_f = 40$ cm/s and $S_r = 10$ cm/s respectively, a bulk lifetime of $\tau_b = 500$ µs and a thickness of $W = 120$ µm and for a low quality wafer featuring $S_f = 40$ cm/s, $S_r = 150$ cm/s, $\tau_b = 50$ µs and $W = 200$ µm. We assume an excess carrier generation by 800 nm light with an intensity of 0.1 suns. We deem these parameters to represent typical passivated wafers with extreme differences in carrier profiles in a reasonable way. The simulated profiles are shown in Fig. 7 b). In order to estimate the differences in calibration factors caused by these differences in carrier profile depth dependence, we compute the integral in equation **(1)** inserting the simulated excess carrier densities to equation **(4)**. We find that the ratio in the resulting calibration

constants is 0.968. Since the chosen parameters represent extreme cases it can be concluded that depth dependent carrier profiles cause errors smaller than 4 %. Hence these errors could be in the dominating regime for certain cases of samples, but are still uncritical if an error margin of 10 % is aimed at by the PLI-PC approach.

5.3. Uncertainties in other quantities

A comprehensive analysis on uncertainties of all quantities entering into the PLI-PC calculations is beyond the scope of this work. Nevertheless other effects should be summarized qualitatively. The spectral uncertainty of *filter transmittances* and *detector sensitivity* of the PLI-setup in use propagate to the thickness weighting function and in second order on the impact of internal optical parameters but no significant impact on the distribution of calibration factors is observed if these quantities are allowed to vary within a reasonable range. Equation **(4)** assumes that the coefficient of radiative recombination does not depend on the injection level. One could argue that this could be a source for uncertainty if the injection level of calibration wafers and test wafers highly vary from each other. Nevertheless the injection levels during the PLI measurement of the above samples are all well below $5{\cdot}10^{14}$ 1/cm^3. According to [12] the changes in the coefficient of radiative recombination are well below 5 % for these injection levels. The effective thickness enhancement due to that fact of a non-zero *angle of light propagation* θ within the sample would lead to a 'bending' of the weighting function $f(W)$. It has been shown in [25] that in samples with a random pyramid texture most of the light leaving the sample vertically to the sample's surface travels at an angle of roughly 39° within the sample. Nevertheless we find that regarding this effective thickness enhancement with respect to the weighting function does not change the distribution of calibration factors significantly (the relative standard deviation of the distribution changes from 4.27 % to 4.30 %). *Parasitic signals* which add up to the detected PLI signal as an offset could be causing changes in calibration factors. For the setup in use the parasitic signal is well below 8 counts/s. The sample emitting the lowest luminescence signal in the investigated sample set featured a luminescence signal of 150 counts/s. An error well below 5 % is hence expected to be caused by parasitic signal. The parasitic signal could nevertheless become a dominating effect if samples with very low lifetimes are used as calibration samples for very high lifetime test wafers. The uncertainty of the *PC sensor sensitivity function* might have an impact if the lifetime distributions of test and calibration wafer are extremely different within the region of coil sensitivity. We varied the radius of the assumed sensitivity function from 6 mm to 12 mm in 0.5 mm steps and the width of the sensitivity function from 2.5 mm to 5 mm in 0.25 mm steps. For each of the 28 samples we extracted weighted PL signals ϕ for every combination of radius and width. This is quite an extreme variation and hence leads to a very conservative estimation of uncertainty caused by improper knowledge of the coil sensitivity region. The standard deviations of the extracted values for the weighted PL signals are a measure for the uncertainty caused by the uncertainty of coil sensitivity. For the 28 test samples we find the highest standard deviation to be 4.5 % and the lowest one to be 1 %. This can lead to the conclusion that uncertainties in the coil response could in extreme cases move into the dominating uncertainty regime.

6. Discussion and rules of thumb

PLI measurements need to be conducted under low irradiation in order to maintain low or at least moderate injection levels. As a pragmatic choice an irradiation of 0.1 suns ($2.5{\cdot}10^{16}\frac{\text{photons}}{\text{s}\cdot\text{cm}^2}$) is recommended, which will most likely assure low level injections for all typical samples.

The delimiting factor in the accuracy of the PLI-PC approach originates from differences in the calibration factor between calibration and test sample. It is hence strongly advised to use calibration wafers which are similar to the wafer under test. There is no hard definition for this similarity, but a few factors can easily be regarded:

The thickness should be equal. Since thickness can easily be measured this is simple to realize experimentally if suitable wafers are available. If they are not available, the thickness weighting function should be regarded, which nevertheless requires detailed knowledge about the PLI-setup in use.

Optical properties should be similar. As a thumb rule a similar optical appearance to the eye is a very good indication. A further recommended measure is to assure that calibration wafers and test wafers were textured by the same texturing processes. Comparing for example KOH textured samples with black silicon textured samples might lead to errors although the optical appearance to the eye is likely to be similar. The impact of internal reflectivities and surface morphologies is not comprehensively investigated in this work, but if suitable filters are used in the PLI-setup, the impact of these will very unlikely cause dominating errors to the method.

Due to uncertainties in the coil sensitivity during the PC measurement strong inhomogeneities in the PL images within the coil region should be avoided in both calibration and test wafers.

The calibration wafers and wafers under test should be measured within a short time interval (ideally the same day) in order to avoid errors due to possible drift of the measurement equipment.

For the chosen set of test samples, which is intentionally chosen *not* to be similar by the above criteria (except for similar front side optics) in order to represent a maximum error that could occur due to an 'unwise' choice of test and calibration samples, the maximum errors produced by PLI-PC are lower than 10 %.

7. Conclusion

We introduced a contactless and non-destructive approach (called PLI-PC) for the determination of base resistivity of wafers featuring highly doped surfaces. We compared the results of the PLI-PC method to inductive measurements after the removal of highly doped layers on a set of test samples. The test samples were chosen after best knowledge in order to represent a wide variety of solar cell precursors used for process optimization in laboratory environments. The experiment showed deviations of less than 10 % from the base resistivity determined by PLI-PC and inductively measured after the removal of highly doped layers. The mean absolute error is below 4 % for the investigated set of samples. A detailed discussion on the impact of depth dependent carrier profiles and wafer optics lead to the conclusion that these factors are not the dominating sources of the remaining uncertainty. From the detailed discussion we derived thumb rules for the conduction of the PLI-PC method and we expect a maximum error lower than 10% if rules of thumb are followed.

Acknowledgements

The authors thank Dirk Wagenmann and the laboratory team at Fraunhofer ISE for the help with sample preparation. For the fruitful discussions the authors specially thank Andreas Fell and David Herrmann. This work was supported by the Federal Ministry for Economic Affairs and Energy within the frame of the project "CUT-B" (0325910A).

References

[1] D.K. Schroder, Semiconductor Material and Device Characterization, third ed., John Wiley & Sons, Hoboken, New Jersey, USA, 2006.
[2] Z. Hameiri, T. Trupke, N. Gao, R.A. Sinton, J.W. Weber, Effective bulk doping concentration of diffused and undiffused silicon wafers obtained from combined photoconductance and photoluminescence measurements, Prog. Photovoltaics Res. Appl. 21 (2013) 942–949.
[3] T. Trupke, R.A. Bardos, M.C. Schubert, W. Warta, Photoluminescence imaging of silicon wafers, Appl. Phys. Lett. 89 (4) (2006) 44107.

[4] R.A. Sinton, A. Cuevas, M. Stuckings, Quasi-steady-state photoconductance, a new method for solar cell material and device characterization, 25th IEEE Photovoltaic Specialists Conference Washington DC, 1996, pp. 457–460 Washington DC.
[5] T. Trupke, et al., Effective excess carrier lifetimes exceeding 100 milliseconds in float zone silicon determined from photoluminescence, 19th EU PVSEC, 2004, pp. 758–761 Paris.
[6] P. Würfel, The chemical potential of radiation, J. Phys. C Solid State Phys. 15 (18) (1982) 3967–3985.
[7] P. Würfel, et al., Diffusion lengths of silicon solar cells from luminescence images, J. Appl. Phys. 101 (12) (2007) 123110.
[8] C. Schinke, D. Hinken, J. Schmidt, K. Bothe, R. Brendel, Modeling the spectral luminescence emission of silicon solar cells and wafers, IEEE J. Photovoltaics 3 (3) (2013) 1038–1052.
[9] K. Schick, E. Daub, S. Finkbeiner, P. Würfel, Verification of a generalized Planck law for luminescence radiation from silicon solar cells, Appl. Phys. A 54 (2) (1992) 109–114.
[10] H.C. Sio, S.P. Phang, T. Trupke, D. Macdonald, An accurate method for calibrating photoluminescence-based lifetime images on multi-crystalline silicon wafers, Sol. Energy Mater. Sol. Cells 131 (2014) 77–84.
[11] C. Schinke, K. Bothe, P. Christian Peest, J. Schmidt, R. Brendel, Uncertainty of the coefficient of band-to-band absorption of crystalline silicon at near-infrared wavelengths, Appl. Phys. Lett. 104 (8) (2014) 81915.
[12] P.P. Altermatt, et al., Injection dependence of spontaneous radiative recombination in crystalline silicon: experimental verification and theoretical analysis: experimental verification and theoretical analysis, Appl. Phys. Lett. 88 (26) (2006) 261901.
[13] H. Nagel, C. Berge, A.G. Aberle, Generalized analysis of quasi-steady-state and quasi-transient measurements of carrier lifetimes in semiconductors, J. Appl. Phys. 86 (11) (1999) 6218–6221.
[14] J.A. Giesecke, M.C. Schubert, B. Michl, F. Schindler, W. Warta, Minority carrier lifetime imaging of silicon wafers calibrated by quasi-steady-state photoluminescence, Sol. Energy Mater. Sol. Cells 95 (3) (2011) 1011–1018.
[15] J. Giesecke, Quantitative Recombination and Transport Properties in Silicon from Dynamic Luminescence, Springer, 2014.
[16] D. Kiliani, et al., Minority charge carrier lifetime mapping of crystalline silicon wafers by time-resolved photoluminescence imaging, J. Appl. Phys. 110 (5) (2011) 54508.
[17] D.M. Caughey, R.E. Thomas, Carrier mobilities in silicon empirically related to doping and field, Proc. IEEE 55 (12) (1967) 2192–2193.
[18] F. Schindler, "Electrical Material Properties and Efficiency Limits of Compensated and Multicrystalline Silicon for Solar Cells," Dissertation, Fakultät für Angewandte Wissenschaften, Albert-Ludwigs-Universität Freiburg, Freiburg im Breisgau, 2015.
[19] R.C. Newman, Thermal donors in silicon: oxygen clusters or self-interstitial aggregates, J. Phys. C Solid State Phys. 18 (30) (1985) 967–972.
[20] K.R. McIntosh, R.A. Sinton, Uncertainty in photoconductance lifetime measurements that use an inductive-coil detector, 23rd EU PVSEC, 2008, pp. 77–82 Valencia.
[21] R. Brendel, M. Hirsch, R. Plieninger, J.H. Werner, Quantum efficiency analysis of thin-layer silicon solar cells with back surface fields and optical confinement, IEEE Trans. Electron Devices 43 (7) (1996) 1104–1113 http://ieeexplore.ieee.org/ielx1/16/10982/00502422.pdf?tp=&arnumber=502422&isnumber=10982.
[22] P.A. Basore, Extended spectral analysis of internal quantum efficiency, 23rd IEEE Photovoltaic Specialists Conference Louisville, 1993, pp. 147–152 Louisville.
[23] J. Müller, K. Bothe, S. Herlufsen, T. Ohrdes, R. Brendel, Reverse saturation current density imaging of highly doped regions in silicon employing photoluminescence measurements, IEEE J. Photovoltaics 2 (4) (2012) 473–478.
[24] D. Hinken, K. Bothe, K. Ramspeck, S. Herlufsen, R. Brendel, Determination of the effective diffusion length of silicon solar cells from photoluminescence, J. Appl. Phys. 105 (10) (2009) 104516.
[25] S. Baker-Finch, K.R. McIntosh, Reflection of normally incident light from silicon solar cells with pyramidal texture, Prog. Photovoltaics Res. Appl. 19 (4) (2011) 406–416.